Multiscale modelling of titanium aluminides

Arjen Roos, Jean-Louis Chaboche, Lionel Gélébart, Jérôme Crépin

Multiscale modelling of titanium aluminides

A. Roos[a,*], J.-L. Chaboche[a], L. Gélébart[b], J. Crépin[b]

[a]*ONERA DMSE/LCME, 29 Avenue de la Division Leclerc, BP72 F-92322 Châtillon cedex, France*
[b]*Ecole Polytechnique LMS (UMR CNRS 7649) 91128 Palaiseau cedex, France*

Abstract

In this work a three-scale model of the mechanical behaviour of titanium aluminides is presented. The first scale transition between the macroscopic length scale and the scale of an individual α_2, γ or lamellar $\alpha_2 + \gamma$ grain is made using elastically self-consistent transformation field analysis (TFA) with anisotropic elasticity. The constitutive equations of the α_2 and γ-phases are obtained through the framework of crystal plasticity. The effective behaviour of the lamellar α_2–γ phase, however, necessitates a second scale transition. This transition, derived from a system of linear equations for a multilayer, is obtained and shown to be equivalent to the formalism of transformation field analysis. Some simple simulations are presented to show the viability of the method.

Keywords: B. Anisotropic material; B. Constitutive behaviour; B. Polycrystalline material; C. Analytic functions; Multiscale model

1. Introduction

Titanium aluminides have been subject of an immense research effort for the last decade and a half. Experimental and theoretical papers have been written ranging from the macroscopic length scale through the length scale of dislocations down to the length scale of atoms, for instance, Yoo et al. (1991, 1995), Inui et al. (1992, 1995), Schlögl (1997), Zghal et al. (1997), Kishida et al. (1998), Morvan and Chaboche (1999), Werwer and Cornec (2000), Gélébart (2002), Brockman (2003) and Marketz et al. (2003). This interest has been sparked by its promising mechanical properties, such as high strength, low density and

* Corresponding author.
E-mail address: arjen.roos@onera.fr (A. Roos).

excellent creep resistance at high temperatures. As such, it is of special interest to the aerospace and automotive industries.

This paper focuses on the effective mechanical properties of intermetallic titanium aluminides near the stoichiometric TiAl composition. The solid phases of interest are the α_2 phase and the γ phase. The first is a disordered Ti_3Al phase with a DO_{19} structure. The γ phase is an ordered TiAl phase composed of alternate layers of Al and Ti atoms ($L1_0$-structure).

Depending on the processing and thermal history, the following microstructures are observed (Schlögl, 1997): the *near gamma* (NG) microstructure with mostly equiaxed γ-TiAl grains with relatively small α_2-Ti_3Al grains inbetween. The *duplex* microstructure consists of interspersed γ-TiAl, and *lamellar* grains of roughly the same size. The lamellar grains consists of fine sheets of α_2-Ti_3Al and γ-TiAl, with thicknesses down to several tens of nanometers. In the *near lamellar* (NL) microstructure the large lamellar grains have the largest volume fraction, but there are still some small grains of γ-TiAl present. Finally, the *fully lamellar* (FL) phase consists of very large (of the order of 100 μm) lamellar grains.

These microstructures suggest some typical length scales on which to base our modelling efforts. The first is the *macroscale* of the structure on which we want to carry out our calculations. Then, a transition is made to the *mesoscale*, which consist of individual grains: the α_2 grains, the γ grains and the lamellar grains. Finally, the *microscale* presents itself as the scale of individual lamellae or domains of the lamellar grain.

The constitutive laws of the individual α_2 and γ grains (on the mesoscopic length scale) and of the individual layers in the lamellar grains (on the microscopic length scale) are described using crystal plasticity. It can be argued that by using crystal plasticity (as in this paper), another scale transition is made to a "nanoscale" when the stress within a grain or domain is projected onto an individual slip plane, and when the resulting strain (rate) on each slip plane is homogenised to the whole grain or domain. However, we will leave this discussion open and will proceed with *three* length scales: macro–meso–micro.

The organisation of this paper is as follows: first, the general methods of transformation fields analysis and crystal plasticity are briefly recalled (Section 2). Then, in Section 3, these methods are applied to the specific case of the microstructure of TiAl to obtain a mechanical model on three length scales. Section 4 presents some simulations on the meso→micro transition and the full three-scale model, respectively. The paper is concluded by Section 5.

2. Scale change—methods

In order to introduce the relevant concepts and quantities, this section will briefly recall the method of *transformation field analysis* (TFA) and its application to the *elastically self-consistent* case. The section finishes with *crystalline plasticity*, a method which describes the effective deformation of a crystal, and its evolution due to dislocation motion on its slip planes.

2.1. Transformation field analysis (TFA)

This method is based on the idea of a purely elastic redistribution of the macroscopic stress and strain, and of the local eigenstresses or eigenstrains. According to Dvorak and Benveniste (1992), a *phase* is defined as an elastically homogeneous part of the representative volume; no limitations are placed on phase geometry or elastic symmetry, except that the latter remains fixed in the overall coordinate system. In this work, the term *subvolume* will be used instead to distinguish from the material *phase*.

The volume fraction of a subvolume i is written as c^i, its volume as V^i, its stiffness as $\underset{\approx}{\mathbf{L}}^i$ (or its compliance $\underset{\approx}{\mathbf{M}}^i \equiv \underset{\approx}{\mathbf{L}}^{i-1}$), the stress whithin the subvolume (which may depend on the position $\vec{x}$ within the subvolume) as $\underset{\sim}{\sigma}^i\left(\vec{x}\right)$ and the total strain within the subvolume as $\underset{\sim}{\varepsilon}^i\left(\vec{x}\right)$. Finally, the eigenstress within the subvolume is $\underset{\sim}{\lambda}^i\left(\vec{x}\right)$ and the eigenstrain within the subvolume is $\underset{\sim}{\mu}^i\left(\vec{x}\right)$.

2.1.1. TFA—general framework

At the macroscale, the uniform stress $\underset{\sim}{\mathbf{\Sigma}}$ and uniform strain $\underset{\sim}{\mathbf{E}}$ are related through Hooke's law,

$$\underset{\sim}{\mathbf{\Sigma}} = \underset{\approx}{\mathbf{L}} : \underset{\sim}{\mathbf{E}} + \underset{\sim}{\lambda} \tag{1}$$

$$\underset{\sim}{\mathbf{E}} = \underset{\approx}{\mathbf{M}} : \underset{\sim}{\mathbf{\Sigma}} + \underset{\sim}{\mu} \tag{2}$$

with $\underset{\approx}{\mathbf{L}}$ the macroscopic stiffness, $\underset{\approx}{\mathbf{M}} \equiv \underset{\approx}{\mathbf{L}}^{-1}$, $\underset{\sim}{\lambda}$ the macroscopic eigenstress and $\underset{\sim}{\mu}$ the macroscopic eigenstrain. Between the latter quantities we have

$$\underset{\sim}{\lambda} = -\underset{\approx}{\mathbf{L}} : \underset{\sim}{\mu} \tag{3}$$

Hooke's law also holds in each subvolume i:

$$\underset{\sim}{\sigma}^i(\vec{x}) = \underset{\approx}{\mathbf{L}}^i : \underset{\sim}{\varepsilon}^i(\vec{x}) + \underset{\sim}{\lambda}^i(\vec{x}) \tag{4}$$

$$\underset{\sim}{\varepsilon}^i(\vec{x}) = \underset{\approx}{\mathbf{M}}^i : \underset{\sim}{\sigma}^i(\vec{x}) + \underset{\sim}{\mu}^i(\vec{x}) \tag{5}$$

with $\underset{\approx}{\mathbf{M}}^i \equiv \left(\underset{\approx}{\mathbf{L}}^i\right)^{-1}$, and no implicit summation is implied by repeated indices. Again,

$$\underset{\sim}{\lambda}^i(\vec{x}) = -\underset{\approx}{\mathbf{L}}^i : \underset{\sim}{\mu}^i(\vec{x}) \tag{6}$$

Starting with the assumption that the eigenstrains and eigenstresses are uniform in each subvolume i, which will be denoted by $\underset{\sim}{\mu}^i$ and $\underset{\sim}{\lambda}^i$ respectively, the TFA localisation equations are

$$\underset{\sim}{\varepsilon}^i(\vec{x}) = \underset{\approx}{\mathbf{A}}^i(\vec{x}) : \underset{\sim}{\mathbf{E}} + \sum_{j=1}^{N} \underset{\approx}{\mathbf{D}}^{ij}(\vec{x}) : \underset{\sim}{\mu}^j \tag{7}$$

$$\underset{\sim}{\sigma}^i(\vec{x}) = \underset{\approx}{\mathbf{B}}^i(\vec{x}) : \underset{\sim}{\mathbf{\Sigma}} + \sum_{j=1}^{N} \underset{\approx}{\mathbf{F}}^{ij}(\vec{x}) : \underset{\sim}{\lambda}^j \tag{8}$$

which introduces several quantities. The tensors $\underset{\approx}{\mathbf{A}}^i(\vec{x})$ and $\underset{\approx}{\mathbf{B}}^i(\vec{x})$ are called the strain concentration factors and stress concentration factors, respectively. They are related through

$$\underset{\approx}{\mathbf{L}}^i : \underset{\approx}{\mathbf{A}}^i(\vec{x}) = \underset{\approx}{\mathbf{B}}^i(\vec{x}) : \underset{\approx}{\mathbf{L}} \tag{9}$$

and their averages over the subvolume i are denoted by $\underset{\approx}{\mathbf{A}}^i$ and $\underset{\approx}{\mathbf{B}}^i$. The $\underset{\approx}{\mathbf{D}}^{ij}(\vec{x})$ are the eigenstrain influence functions, which is called self-induced for $i=j$ and transmitted for $i \neq j$. The $\underset{\approx}{\mathbf{F}}^{ij}(\vec{x})$ are the corresponding eigenstress influence functions. Their averages on the subvolume i are known as the eigenstrain concentration factors $\underset{\approx}{\mathbf{D}}^{ij}$ and the eigenstress concentration factors $\underset{\approx}{\mathbf{F}}^{ij}$. Note that the localisation equation for the stress can also be written in terms of the eigenstrains $\underset{\sim}{\mu}^j$ by using Eq. (6). For later use, we define $\underset{\approx}{\mathbf{Q}}^{ij} \equiv \underset{\approx}{\mathbf{F}}^{ij} : \underset{\approx}{\mathbf{L}}^j$.

Assuming uniform eigenstress in subvolume i, the macroscopic stress $\underset{\sim}{\mathbf{\Sigma}}$ and strain $\underset{\sim}{\mathbf{E}}$ are given by the averages

$$\underset{\sim}{\mathbf{\Sigma}} \equiv \left\langle \underset{\sim}{\sigma} \right\rangle = \sum_i c^i \underset{\sim}{\sigma}^i \text{ and } \underset{\sim}{\mathbf{E}} \equiv \left\langle \underset{\sim}{\varepsilon} \right\rangle = \sum_i c^i \underset{\sim}{\varepsilon}^i \tag{10}$$

where

$$\underset{\sim}{\sigma}^i = \frac{1}{V^i} \int_{V^i} \underset{\sim}{\sigma}^i(\vec{x}) \mathrm{d}\vec{x} \text{ and } \underset{\sim}{\varepsilon}^i = \frac{1}{V^i} \int_{V^i} \underset{\sim}{\varepsilon}^i(\vec{x}) \mathrm{d}\vec{x} \tag{11}$$

denote the averages over the subvolumes i. Similarly, we have

$$\underset{\sim}{\lambda} = \sum_i c^i \underset{\approx}{\mathbf{A}}^{i^T} : \underset{\sim}{\lambda}^i, \underset{\sim}{\mu} = \sum_i c^i \underset{\approx}{\mathbf{B}}^{i^T} : \underset{\sim}{\mu}^i \tag{12}$$

and

$$\underset{\approx}{\mathbf{L}} = \sum_i c^i \underset{\approx}{\mathbf{L}}^i : \underset{\approx}{\mathbf{A}} \tag{13}$$

2.1.2. Elastic selfconsistent TFA

In the self-consistent method, the equivalent homogeneous medium, as seen by each subvolume, is an average of all subvolumes. In our case, we choose an average involving elastic properties only, but without any restrictions on the type of elasticity. We show that in some special cases the TFA localisation equation reduces exactly to the Kröner localisation equation.

The equivalent homogeneous medium is characterised by its stiffness $\underset{\approx}{\mathbf{L}}$ according to Eq. (13). For this particular case

$$\underset{\approx}{\mathbf{A}}^{i} = \left(\underset{\approx}{\mathbf{L}}^{*} + \underset{\approx}{\mathbf{L}}^{i}\right)^{-1} : \left(\underset{\approx}{\mathbf{L}}^{*} + \underset{\approx}{\mathbf{L}}\right) \tag{14}$$

$$\underset{\approx}{\mathbf{B}}^{i} = \left(\underset{\approx}{\mathbf{M}}^{*} + \underset{\approx}{\mathbf{M}}^{i}\right)^{-1} : \left(\underset{\approx}{\mathbf{M}}^{*} + \underset{\approx}{\mathbf{M}}\right) \tag{15}$$

with $\underset{\approx}{\mathbf{L}}^{*} = \underset{\approx}{\mathbf{L}}^{*}\left(\underset{\approx}{\mathbf{L}}\right)$ Hill's constraint tensor of the ellipsoid transformed homogeneous inclusion. For media with aligned inclusions of similar shape, there is only a single $\underset{\approx}{\mathbf{L}}^{*}$. The transformation influence tensors then become

$$\underset{\approx}{\mathbf{D}}^{ij} = \left(\underset{\approx}{\mathbf{I}} - \underset{\approx}{\mathbf{A}}^{i}\right) : \left(\underset{\approx}{\mathbf{L}}^{i} - \underset{\approx}{\mathbf{L}}\right)^{-1} : \left(\delta_{ij}\underset{\approx}{\mathbf{I}} - c^{j}\underset{\approx}{\mathbf{A}}^{j^{T}}\right) : \underset{\approx}{\mathbf{L}}^{j} \tag{16}$$

$$\underset{\approx}{\mathbf{F}}^{ij} = \left(\underset{\approx}{\mathbf{I}} - \underset{\approx}{\mathbf{B}}^{i}\right) : \left(\underset{\approx}{\mathbf{M}}^{i} - \underset{\approx}{\mathbf{M}}\right)^{-1} : \left(\delta_{ij}\underset{\approx}{\mathbf{I}} - c^{j}\underset{\approx}{\mathbf{B}}^{j^{T}}\right) : \underset{\approx}{\mathbf{M}}^{j}, \tag{17}$$

or, written in a different form,

$$\underset{\approx}{\mathbf{D}}^{ij} = \left[\delta_{ij}\underset{\approx}{\mathbf{I}} - c^{j}\left(\underset{\approx}{\mathbf{L}}^{*} + \underset{\approx}{\mathbf{L}}^{i}\right)^{-1} : \left(\underset{\approx}{\mathbf{L}}^{*} + \underset{\approx}{\mathbf{L}}\right)\right] : \left(\underset{\approx}{\mathbf{L}}^{*} + \underset{\approx}{\mathbf{L}}^{j}\right)^{-1} : \underset{\approx}{\mathbf{L}}^{j} \tag{18}$$

$$\underset{\approx}{\mathbf{F}}^{ij} = \left[\delta_{ij}\underset{\approx}{\mathbf{I}} - c^{j}\left(\underset{\approx}{\mathbf{M}}^{*} + \underset{\approx}{\mathbf{M}}^{i}\right)^{-1} : \left(\underset{\approx}{\mathbf{M}}^{*} + \underset{\approx}{\mathbf{M}}\right)\right] : \left(\underset{\approx}{\mathbf{M}}^{*} + \underset{\approx}{\mathbf{M}}^{j}\right)^{-1} : \underset{\approx}{\mathbf{M}}^{j}. \tag{19}$$

It should be stressed that there is no direct link between the shape of the inclusions and the geometry of the actual grains. Rather, for certain spatial distributions of the inclusions it can be shown that the homogenisation problem is formally equivalent to the classical Eshelby problem of an inclusion in an infinite medium (Bornert et al., 2001). The shape of this inclusion derives from the spatial distribution of the grains. Specifically, an isotropic distribution leads to equations equivalent to those of spherical inclusions. In the following, whenever reference is made to the shape of an inclusion in the self-consistent case, it should be interpreted in this manner.

By substituting (17) into Eq. (8), and writing plastic strains $\underset{\sim}{\mathbf{E}}^{\mathrm{p}}$ and $\underset{\sim}{\varepsilon}^{\mathrm{p},i}$ instead of the more general eigenstrains $\underset{\sim}{\mu}$ and $\underset{\sim}{\mu}^{i}$ respectively, and using Eq. (6) we obtain

$$\underset{\sim}{\sigma}^{i} = \underset{\approx}{\mathbf{B}}^{i} : \underset{\sim}{\Sigma} + \left(\underset{\approx}{\mathbf{I}} - \underset{\approx}{\mathbf{B}}^{i}\right) : \left(\underset{\approx}{\mathbf{M}}^{i} - \underset{\approx}{\mathbf{M}}\right)^{-1} : \left(\underset{\sim}{\mathbf{E}}^{\mathrm{p}} - \underset{\sim}{\varepsilon}^{\mathrm{p},i}\right), \tag{20}$$

which is an extension of an existing expression for two phases (Suquet, 1997). Using the alternative expression (19) for $\underset{\approx}{\mathbf{F}}^{ij}$ to substitute in Eq. (8), we can rewrite this as

$$\underset{\sim}{\sigma}^{i} = \underset{\approx}{\mathbf{B}}^{i} : \underset{\sim}{\mathbf{\Sigma}} + \left(\underset{\approx}{\mathbf{M}}^{*} + \underset{\approx}{\mathbf{M}}^{i}\right)^{-1}\left[\left(\underset{\approx}{\mathbf{M}}^{*} + \underset{\approx}{\mathbf{M}}\right) : \sum_{j=1}^{N}\left(c^{j}\left(\underset{\approx}{\mathbf{M}}^{*} + \underset{\approx}{\mathbf{M}}^{j}\right)^{-1} : \underset{\sim}{\varepsilon}^{\mathrm{p},j}\right) - \underset{\sim}{\varepsilon}^{\mathrm{p},i}\right]. \tag{21}$$

As will be shown below, the last two equations can be seen as a direct generalisation of localisation equations of the form

$$\underset{\sim}{\sigma}^{i} = \underset{\sim}{\mathbf{\Sigma}} + \alpha\mu\left(\underset{\sim}{\mathbf{E}}^{\mathrm{p}} - \underset{\sim}{\varepsilon}^{\mathrm{p},i}\right) \tag{22}$$

with μ the shear modulus and α a scalar. Some classical methods can be written in this form (Cailletaud, 1987). For instance, $\alpha \simeq 0$ is called the Sachs model, $\alpha \simeq 2$ is the Lin–Taylor model and in the self-consistent Kröner model

$$\alpha = \frac{2}{15}\frac{7-5\nu}{1-\nu}. \tag{23}$$

which yields $\alpha \simeq 1$ for $\nu \simeq 0.3$. However, all these models are valid only for homogeneous local elasticity and an overall isotropic elastic behaviour.

Hill's constraint tensor $\mathbf{L}^{*}$ can be obtained through the polarisation tensor $\underset{\approx}{\mathbf{P}}$ to which it is related through (Bornert et al., 2001).

$$\underset{\approx}{\mathbf{L}}^{*} = \underset{\approx}{\mathrm{P}}^{-1} - \underset{\approx}{\mathbf{L}}. \tag{24}$$

with

$$\underset{\approx}{\mathbf{P}} = \frac{1}{4\pi\left|\underset{\sim}{\zeta}\right|}\int_{\|\vec{x}\|=1}\frac{\left[\vec{x}\otimes\left(\vec{x}\cdot\underset{\approx}{\mathbf{L}}\cdot\vec{x}\right)^{-1}\otimes\vec{x}\right]^{(\mathrm{s})}}{\left\|\underset{\sim}{\zeta}^{-1}\cdot\vec{x}\right\|^{3}}\mathrm{d}S(\vec{x}). \tag{25}$$

Here $\vec{x}$ denotes the position vector and the symbol $^{(\mathrm{s})}$ denotes a double symmetrisation of a fourth order tensor according to

$$A^{(\mathrm{s})}_{ijkl} = \frac{1}{4}\left(A_{ijkl} + A_{jikl} + A_{ijlk} + A_{jilk}\right). \tag{26}$$

The second order tensor $\underset{\sim}{\zeta}$ decribes the geometry of the ellipsoid according to $\left\|\underset{\sim}{\zeta}\cdot\vec{x}\right\| = R$. For an unit sphere ($R=1$), Eq. (25) simplifies to

$$\underset{\approx}{\mathbf{P}} = \frac{1}{4\pi}\int_{\|\vec{x}\|=1}\left[\vec{x}\otimes\left(\vec{x}\cdot\underset{\approx}{\mathbf{L}}\cdot\vec{x}\right)^{-1}\otimes\vec{x}\right]^{(s)}\mathrm{d}S(\vec{x}) \tag{27}$$

and for a unit sphere with isotropic elasticity (shear modulus μ, Poisson ratio ν) an analytical solution exists:

$$\underset{\approx}{\mathbf{L}}^{*} = 4\mu\underset{\approx}{\mathbf{J}} + \frac{\mu}{3}\frac{7-5\nu}{4-5\nu}\underset{\approx}{\mathbf{K}} \tag{28}$$

where $\underset{\approx}{\mathbf{J}}$ and $\underset{\approx}{\mathbf{K}}$ are the fourth order dilational and deviatoric projectors, respectively.

In the special case where all inclusions have the same tensor of elasticity, the homogeneous equivalent medium must reflect this, so $\underset{\approx}{\mathbf{L}} = \underset{\approx}{\mathbf{L}}^{i}$ for all i. The mechanical concentration factors then reduce to unity, Eqs. (18) and (19) become

$$\underset{\approx}{\mathbf{D}}^{ij} = \left(\delta_{ij} - c^{j}\right)\left(\underset{\approx}{\mathbf{L}}^{*} + \underset{\approx}{\mathbf{L}}\right)^{-1} : \underset{\approx}{\mathbf{L}} \tag{29}$$

$$\underset{\approx}{\mathbf{F}}^{ij} = \left(\delta_{ij} - c^{j}\right)\left(\underset{\approx}{\mathbf{M}}^{*} + \underset{\approx}{\mathbf{M}}\right)^{-1} : \underset{\approx}{\mathbf{M}} \tag{30}$$

and the stress in subvolume i [Eq. (21)] becomes

$$\underset{\sim}{\sigma}^{i} = \underset{\sim}{\Sigma} + \left(\underset{\approx}{\mathbf{M}}^{*} + \underset{\approx}{\mathbf{M}}\right)^{-1} : \left(\underset{\sim}{\mathbf{E}}^{\mathrm{p}} - \underset{\sim}{\varepsilon}^{\mathrm{p},i}\right). \tag{31}$$

When all inclusions are unit spheres (i.e. arising from an isotropic spatial distribution) with isotropic elasticity, Eq. (21) becomes even more simple by using Eq. (28):

$$\underset{\sim}{\sigma}^{i} = \underset{\sim}{\Sigma} + \mu\left(\frac{4}{3}\frac{1+\nu}{1-\nu}\underset{\approx}{\mathbf{J}} + \frac{2}{15}\frac{7-5\nu}{1-\nu}\underset{\approx}{\mathbf{K}}\right) : \left(\underset{\sim}{\mathbf{E}}^{\mathrm{p}} - \underset{\sim}{\varepsilon}^{\mathrm{p},i}\right). \tag{32}$$

Note that in case of a deviatoric strain state we are left with

$$\underset{\sim}{\sigma}^{i} = \underset{\sim}{\Sigma} + \frac{2}{15}\frac{7-5\nu}{1-\nu}\mu\left(\underset{\sim}{\mathbf{E}}^{\mathrm{p}} - \underset{\sim}{\varepsilon}^{\mathrm{p},i}\right), \tag{33}$$

which shows that for isotropic elasticity and spherical inclusions, self-consistent TFA reduces *exactly* to the Kröner expression.

It is known that a Kröner localisation gives a response that is too stiff. Instead of using a fully incremental Hill approach, it is possible to define a correction method to the TFA (Chaboche et al., 2001). Another approach (Cailletaud, 1987) is to replace the quantities $\underset{\sim}{\mathbf{E}}^{\mathrm{p}}$ and $\underset{\sim}{\varepsilon}^{\mathrm{p}}$ in Eq. (22) by the quantities $\underset{\approx}{\mathbf{B}}$ and $\underset{\sim}{\beta}^{i}$, according to

$$\dot{\underset{\sim}{\beta}}^i = \dot{\underset{\sim}{\varepsilon}}^{\mathrm{p},i} - D\underset{\sim}{\beta}^i \left\| \dot{\underset{\sim}{\varepsilon}}^{\mathrm{p},i} \right\| \text{ and } \underset{\sim}{\boldsymbol{B}} = \sum_i c^i \underset{\approx}{\mathbf{B}}^{i^T} : \underset{\sim}{\beta}^i \tag{34}$$

where D is a phenomenological parameter and $\mathbf{B}^i$ is the stress concentration factor of subvolume i. This correction, also known as the beta-rule, can be applied without modification into Eq. (20).

2.2. Crystal plasticity

Consider a crystalline grain containing a set of slip systems α with slip directions $\vec{l}$ slip plane normals $\vec{n}$, and Schmid tensors

$$\underset{\sim}{\mathbf{m}}_\alpha = \left(\vec{n}_\alpha \otimes \vec{l}_a + \vec{l}_a \otimes \vec{n}_\alpha\right)/2. \tag{35}$$

Then for the shear strain rate $\underset{\sim}{\varepsilon}^g$ under an applied stress $\underset{\sim}{\sigma}^g$ the following expression can be written for each grain (Cailletaud, 1987) (small deformations):

$$\dot{\underset{\sim}{\varepsilon}}^g = \sum_\alpha \dot{\gamma}_\alpha \underset{\sim}{\mathbf{m}}_\alpha, \qquad \dot{\gamma}_\alpha = \operatorname{sign}\left(\underset{\sim}{\sigma}^g : \underset{\sim}{\mathbf{m}}_\alpha\right)\dot{\upsilon}_\alpha, \tag{36}$$

$$\dot{\upsilon}_\alpha = \left\langle \frac{\left|\underset{\sim}{\sigma}^g : \underset{\sim}{\mathbf{m}}_\alpha\right| - r_\alpha}{K} \right\rangle^n, \qquad r_\alpha = r_0 + Q\sum_\beta h_{\alpha\beta}\left(1 - \mathrm{e}^{-b\upsilon_\beta}\right), \tag{37}$$

where the symbol $\langle\cdot\rangle$ denotes the positive part of its argument. The parameters n and K define a Norton-type law. The quantity r_α takes the role of the critical resolved shear stress on slip system α, whose evolution is governed by the parameters Q and b and the hardening matrix $h_{\alpha\beta}$. Alternatively, a linear dependence $h_{\alpha\beta}\upsilon_\beta$ may be used.

The slip systems in titanium aluminides have been described elsewhere (Kishida et al., 1998), so we only give a brief summary here. In the γ phase, deformation takes place on octahedral planes. Due to the ordered structure not all directions are equivalent: depending on the direction, glide consists of $\frac{1}{2}\langle 1\bar{1}0]\{111\}$ dislocations (where the Burgers vector connects two nearest neighbours of the same species, hence the name *normal dislocations*) and of $\langle 01\bar{1}]\{111\}$ superdislocations (where along the Burgers vector the nearest neighbours are of different species, so in order to leave the lattice invariant, twice the distance has to be traversed as for the normal dislocations). An important deformation mode is (unidirectional) $\frac{1}{2}\langle 11\bar{2}]\{111\}$ twinning. In the $\alpha 2$ phase, the deformation modes are basal $(0001)\left\langle 11\bar{2}0\right\rangle$ slip, prism $\left\{1\bar{1}00\right\}\left\langle 11\bar{2}0\right\rangle$ slip and pyramidal $\left\{11\bar{2}1\right\}\left\langle \bar{1}\bar{1}26\right\rangle$ $(2\mathrm{c}+a)$ slip.

In the lamellar phase, the small thickness of the lamellae induces confinement effects, such as the Hall–Petch effect, that can not be taken into account using classical continuum mechanics. This is taken into account by multiplying the r_0 and Q by a morphological parameter, depending on whether the slip plane and Burgers vector both lie in the habit plane of the lamellae (*longitudinal slip*), or only the slip plane lies in the habit plane (*mixed slip*), or neither (*tranverse slip*).

3. Three-scale model

3.1. Macro→meso→macro

From the morphology of the microstructures generally found in the titanium aluminides of our interest, we assume the following: there is no preferential geometrical orientation, i.e. the distribution of the grains is isotropic. Furthermore, no type of grain and orientation can be seen to be sufficiently dominant to be considered as a matrix in which the other grains are embedded, so that we cannot approach this problem in the dilute limit.

Based on these assumptions we apply elastically self-consistent TFA: no phase is preferred and all phases see an equivalent homogeneous comparison medium, the matrix. Additionally, this allows for using anisotropic elasticity and crystal plasticity. The constraint of one single Hill tensor $\underset{\approx}{\mathbf{L}}$ for all subvolumes forces us to have a single geometrical shape and alignment of all inclusions. This constraint is satisfied automatically for an isotropic distribution of the grains, because then the problem is formally equivalent to the one of a spherical inclusion. It has the additional advantage that the expression for the polarisation tensor, Eq. (25), simplifies considerably to Eq. (27).

With these assumptions, as depicted schematically in the top part of Fig. 1, we may now collect the appropriate equations from the previous sections. We start by localising the stress at the transition macro→meso using Eq. (20), and homogenising the strain(rate) at the transition meso→macro using Eq. (12). Furthermore, the macroscopic quantities are related through Hooke's law, Eq. (2). So, assuming that we start by applying a macroscopic strain $\underset{\sim}{\mathbf{E}}$, we collect from the following equations (where we use the notation $\underset{\sim}{\mathbf{E}}^{\mathrm{p}}$ and $\underset{\sim}{\varepsilon}^{\mathrm{p},i}$ instead of $\underset{\sim}{\mu}$ and $\underset{\sim}{\mu}^i$, respectively):

$$\text{Hooke} \qquad \underset{\sim}{\mathbf{\Sigma}} = \underset{\approx}{\mathbf{L}} : \left(\underset{\sim}{\mathbf{E}} - \underset{\sim}{\mathbf{E}}^{\mathrm{p}}\right) \tag{38}$$

$$\text{Localise} \qquad \sigma^i = \underset{\approx}{\mathbf{B}}^i : \underset{\sim}{\mathbf{\Sigma}} + \left(\underset{\approx}{\mathbf{I}} - \underset{\approx}{\mathbf{B}}^i\right) : \left(\underset{\approx}{\mathbf{M}}^i - \underset{\approx}{\mathbf{M}}\right)^{-1} : \left(\underset{\sim}{\mathbf{E}}^{\mathrm{p}} - \underset{\sim}{\varepsilon}^{\mathrm{p},i}\right)$$

$$\text{Evolution} \qquad \dot{\gamma}_\alpha^i = \operatorname{sign}\left(\underset{\sim}{\sigma}^i : \underset{\sim}{\mathbf{m}}_\alpha^i\right)\left\langle \frac{\left|\underset{\sim}{\sigma}^i : \underset{\sim}{\mathbf{m}}_\alpha^i\right| - r_\alpha^i}{K_\alpha^i} \right\rangle^{n^i}$$

$$\dot{\gamma}_\alpha^i = \int_0^t \dot{\gamma}_\alpha^i \mathrm{d}t; \; \underset{\sim}{\varepsilon}^{\mathrm{p},i} = \sum_\alpha \gamma_\alpha^i \underset{\sim}{\mathbf{m}}_\alpha^i$$

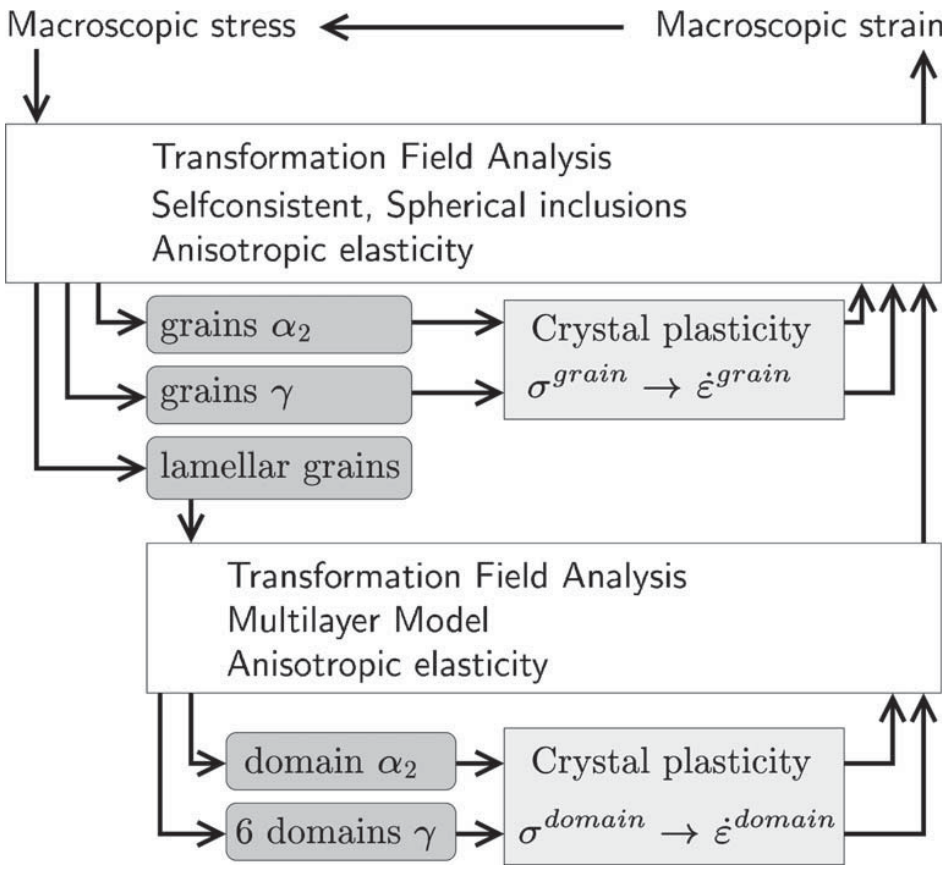

Fig. 1. The three-scale TFA model.

$$\text{Homogenise} \quad \underset{\sim}{\mathbf{E}}^{\mathrm{p}} = \sum_i c^i \underset{\approx}{\mathbf{B}}^{i^T} : \underset{\sim}{\varepsilon}^{\mathrm{p},i}$$

and the corresponding evolution equations of the hardening parameter r_α, in Eq. (37). Notice that not only the eigenstrains $\underset{\sim}{\varepsilon}^{\mathrm{p},i}$ are uniform in each subvolume, but also the stresses $\underset{\sim}{\sigma}^i$. The system of Eq. (38) needs to be solved implicitly for a given $\underset{\sim}{\mathbf{E}}$ at each time increment, because of the dependency of the γ_α^i, on $\underset{\sim}{\sigma}^i$.

We still need to calculate some other quantities: Hooke's law needs the stiffness tensor $\underset{\approx}{\mathbf{L}}$ of the equivalent medium, which depends on all $\underset{\approx}{\mathbf{L}}^i$ and $\underset{\approx}{\mathbf{A}}^i$ [Eq. (13)]. Furthermore, we need $\mathbf{B}^i$. The latter two tensors depend in their turn on $\mathbf{L}^*$, $\mathbf{L}^i$ and $\mathbf{L}$, according to Eqs. (14) and (15). Finally, Hill's constraint tensor $\mathbf{L}^*$ depends on $\mathbf{L}$, according to Eqs. (24) and (27). For clarity, we assemble these equations here:

$$\text{Strain localisation tensor} \quad \underset{\approx}{\mathbf{A}}^i = \left(\underset{\approx}{\mathbf{L}}^* + \underset{\approx}{\mathbf{L}}^i\right)^{-1} : \left(\underset{\approx}{\mathbf{L}}^* + \underset{\approx}{\mathbf{L}}\right) \tag{39}$$

$$\text{Stress localisation tensor} \quad \underset{\approx}{\mathbf{B}}^i = \left(\underset{\approx}{\mathbf{M}}^* + \underset{\approx}{\mathbf{M}}^i\right)^{-1} : \left(\underset{\approx}{\mathbf{M}}^* + \underset{\approx}{\mathbf{M}}\right)$$

$$\text{Overall stiffness} \quad \underset{\approx}{\mathbf{L}} = \sum_i c^i \underset{\approx}{\mathbf{L}}^i : \underset{\approx}{\mathbf{A}}^i$$

$$\text{Hill's tensor} \quad \underset{\approx}{\mathbf{L}}^* = \underset{\approx}{\mathbf{P}}^{-1} - \underset{\approx}{\mathbf{L}}$$

Polarisation tensor $$\underset{\approx}{\mathbf{P}} = \frac{1}{4\pi}\int_{\|\vec{x}\|=1}\left[\vec{x}\otimes\left(\vec{x}\cdot\underset{\approx}{\mathbf{L}}\cdot\vec{x}\right)^{-1}\otimes\vec{x}\right]^{(s)}\mathrm{d}S(\vec{x})$$

Note that $\mathbf{A}^i$ and $\mathbf{B}^i$ are also related through Eq. (9). Due to the self-consistent scheme, this system of equations has to be solved implicitly to obtain $\mathbf{L}$ and $\mathbf{B}^i$ to be used in Eq. (38). However, this has to be done only once, because all tensors in Eq. (39) are unaffected by the evolution equations of Eq. (38).

3.2. *Meso→micro→meso*

In this section we will consider in detail the scale transition from the level of one grain to the level of a representative set of lamellae of the lamellar phase. Several models of the lamellar grain exist in the literature, most notably the work of the research groups of the University of Leoben (Schlögl, 1997), GKSS-Forscbungzentrum Geesthacht (Werwer and Cornec, 2000) and École Polytechnique Palaiseau (Gélébart, 2002). The latter developed a formalism for a scale transition into the lamellar phase (a multilayer model) that we will be following closely. In the same study a comparison was made with a simpler model without scale transition, by using a strongly anisotropic Hill criterion for the onset of plastic flow. There, it has been shown that this criterion cannot describe accurately the surface of plasticity that is given by the multilayer model. In this work, therefore, the formalism of Gélébart is followed. The scale transition that will be developed in this section is depicted schematically in the bottom part of Fig. 1.

The local stresses are obtained through an analytical system of linear equations, where the stresses and strains in each layer are assumed to be constant. This system of equations includes a scale transition explicitly, i.e. the solution of this system of equations is an exact solution of the homogenisation problem. In this case, the approximation is made that since the domain size in the direction parallel to the habit plane (about 50 μm) is much greater than the typical thickness of one lamella (about 1 μm), the domains can be regarded as infinitely long. The lamellae can be represented in a periodic unit cell as in the left part of Fig. 2.

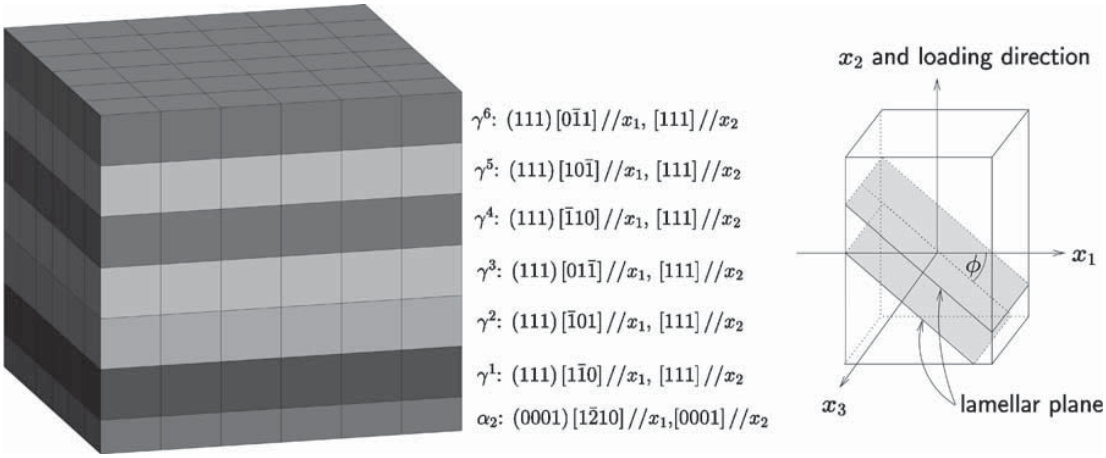

Fig. 2. The lamellar phase. Left: meshed periodic unit cell with orientation relations between the layers, following Kishida et al. (1998). Right: orientation of the periodic unit cell with respect to the loading direction.

Returning now to the formalism of TFA and crystal plasticity, the only assumption that we will make about the lamellar phase is uniform stress $\underset{\sim}{\sigma}^i$ and strain $\underset{\sim}{\varepsilon}^i$ in each domain. Again, because of crystal plasticity, the localisation phase meso→micro will pass through the localisation of stress and the homogeneisation phase micro→meso through the strains. In fact, we can use the same equations (38) as in the previous section, except the localisation of stress, which was written specifically for the self-consistent case, which we clearly cannot apply here. Instead, we take the more general Eq. (8), which we write in terms of the eigenstrains instead of the eigenstresses [using Eq. (6)], and dropping the position dependence within the subvolume.

In order to distinguish from the macro→meso case, it is useful to change our notation slightly. Instead of $\underset{\sim}{\Sigma}$, which traditionally denotes the uniform stress at the higher length scale, we will now use $\underset{\sim}{\sigma}^{\mathrm{g}}$, where the g stands for grain. This reflects the fact that we start from the mesoscopic level of the whole grain, instead of the macroscopic level. Similarly, we will write $\underset{\sim}{\varepsilon}^{\mathrm{g}}$ and $\underset{\sim}{\varepsilon}^{\mathrm{g,p}}$ instead of $\underset{\sim}{\mathbf{E}}$ and $\underset{\sim}{\mathbf{E}}^{\mathrm{p}}$, respectively, and $\mathbf{L}^{\mathrm{g}}$ instead of $\mathbf{L}$. Also, to avoid confusion with the other tensors of the macro →meso transition, we will write a bar over them. On the other hand, all other quantities, referred to by a superscript or subscript i or j, are understood to be at the microscopic level, i.e. belonging to domain (subvolume) i or j. We then arrive at

$$\text{Hooke} \qquad \underset{\sim}{\sigma}^{\mathrm{g}} = \underset{\approx}{\mathbf{L}}^{\mathrm{g}} : \left(\underset{\sim}{\varepsilon}^{\mathrm{g}} - \underset{\sim}{\varepsilon}^{\mathrm{g,p}}\right) \tag{40}$$

$$\text{Localise} \qquad \underset{\sim}{\sigma}^i = \underset{\approx}{\bar{\mathbf{B}}}^i : \underset{\sim}{\sigma}^{\mathrm{g}} - \sum_{j=1}^{N} \underset{\approx}{\bar{\mathbf{F}}}^{ij} : \underset{\approx}{\mathrm{L}}^j : \underset{\sim}{\varepsilon}^{\mathrm{p},j}$$

$$\text{Evolution} \qquad \dot{\gamma}_\alpha^i = \operatorname{sign}\left(\underset{\sim}{\sigma}^i : \underset{\sim}{\mathbf{m}}_\alpha^i\right)\left\langle \frac{\left|\underset{\sim}{\sigma}^i : \underset{\sim}{\mathbf{m}}_\alpha^i\right| - r_\alpha^i}{K_\alpha^i} \right\rangle^{n^i}$$

$$\gamma_\alpha^i = \int_0^t \dot{\gamma}_\alpha^i \mathrm{d}t; \qquad \underset{\sim}{\varepsilon}^{\mathrm{p},i} = \sum_\alpha \gamma_\alpha^i \underset{\sim}{\mathbf{m}}_\alpha^i$$

$$\text{Homogenise} \qquad \underset{\sim}{\varepsilon}^{\mathrm{g,p}} = \sum_i c^i \underset{\approx}{\bar{\mathbf{B}}}^{iT} : \underset{\sim}{\varepsilon}^{\mathrm{p},i}$$

and again the corresponding evolution equations for the hardening parameters.

In the macro→meso transition, additional assumptions such as the shape of the inclusions, and the self-consistent homogeneous equivalent medium, were needed to arrive at expressions for the mechanical localisation tensors $\underset{\approx}{\mathbf{A}}^i$ and $\underset{\approx}{\mathbf{B}}^i$, the effective elasticity $\underset{\approx}{\mathbf{L}}$, and the transformation influence tensors $\underset{\approx}{\mathbf{F}}^{ij}$. In this case, however, these assumptions cannot be made and the remaining part of this section is devoted to obtaining expressions through other assumptions.

As a starting point, the multilayer model of Gélébart is closely followed. However, in this paper the stresses and strains are not written in rate form, as in the original model. The equations of the original model can be recovered by writing $\dot{\underset{\sim}{\sigma}}$ and $\dot{\underset{\sim}{\varepsilon}}$

instead of $\underset{\sim}{\sigma}$ and $\underset{\sim}{\varepsilon}$ in Eqs. (41)–(44) below. Furthermore, in the original model the evolution of plastic strain rate as a function of the stress rate and the active deformation systems yields an additional set of *linear* equations, which are then solved simultaneously with the equivalent Eqs. (41)–(44). In this paper, however, we assume that the plastic deformations are known quantities for the localisation step, and the increment of plastic strain is calculated in a separate, subsequent step. In other words, there is an explicit separation between the scale transition and the integration of the constitutive equation of each subvolume. This has the advantage of not being limited to models with linear hardening, although the calculations presented in this paper only use the latter. Otherwise, it can be shown that the two forms are equivalent.

In the multilayer model, the stresses $\underset{\sim}{\sigma}^i$ and strains $\underset{\sim}{\varepsilon}^i$ are assumed to be uniform in each layer. In the following, the components of the second-order stress and strain tensors are stored following the Voigt convention, but with the order of storage $11\rightarrow1$, $22\rightarrow2$, $33\rightarrow3$, $12\rightarrow4$, $23\rightarrow5$, $31\rightarrow6$.

We start with the limiting conditions: the stresses *or* strains of each layer i are homogenised according to the six equations

$$\underset{\sim}{\sigma}^{\mathrm{g}} = \sum_{i=1}^{N} c^i \underset{\sim}{\sigma}^i \qquad \text{or} \qquad \underset{\sim}{\varepsilon}^{\mathrm{g}} = \sum_{i=1}^{N} c^i \underset{\sim}{\varepsilon}^i. \tag{41}$$

At each interface, the transversal components (T, i.e. the components normal to the habit plane) of the stress $(\sigma^i_{33}, \sigma^i_{23}, \sigma^i_{31}) = {}^T\underset{\sim}{\sigma}^i$ should be continuous, which yields $3\cdot(N-1)$ equations for $i = 1\ldots(N-1)$:

$${}^T\underset{\sim}{\sigma}^i = {}^T\underset{\sim}{\sigma}^{i+1} \tag{42}$$

The longitudinal (L, i.e. lying in the habit plane) components of the strain $\left(\varepsilon^i_{11}, \varepsilon^i_{22}, \varepsilon^i_{12}\right) = {}^L\underset{\sim}{\varepsilon}^i$ should satisfy the following $3\cdot(N-1)$ equations, again for $i = 1\ldots(N-1)$:

$${}^L\underset{\sim}{\varepsilon}^i = {}^L\underset{\sim}{\varepsilon}^{i+1} \tag{43}$$

Finally, Hooke's law holds in each layer, yielding $6\cdot N$ equations:

$$\underset{\sim}{\sigma}^i - \underset{\approx}{\mathbf{L}}^i : \underset{\sim}{\varepsilon}^i = -\underset{\approx}{\mathbf{L}}^i : \underset{\sim}{\varepsilon}^{\mathrm{p},i} \tag{44}$$

If we consider the plastic deformations $\underset{\sim}{\varepsilon}^{\mathrm{p},i}$ as known quantities (from the implicit scheme), we have a linear system of $12\cdot N$ equations for $6\cdot N$ unknown $\underset{\sim}{\sigma}^i$ and $6\cdot N$ unknown $\underset{\sim}{\varepsilon}^i$. The remainder of this section gives the analytical solution of this system.

The splitting into transversal (T), i.e. with components in the x_3-direction, and longitudinal (L) parts, i.e. the remaining components can be applied to all tensors of the system of equations to obtain a simplified tation, similar to for instance El Omri et al. (2000) or Stupkiewicz and Petryk (2002). For instance, the tensors of elasticity $\underset{\approx}{\mathbf{L}}^i$ of each layer become 3×3 matrices:

$$
{}^{LL}\mathbf{L}^i = \begin{pmatrix} L^i_{11} & L^i_{12} & L^i_{14} \\ L^i_{21} & L^i_{22} & L^i_{24} \\ L^i_{41} & L^i_{42} & L^i_{44} \end{pmatrix} \quad {}^{LT}\mathbf{L}^i = \begin{pmatrix} L^i_{13} & L^i_{15} & L^i_{16} \\ L^i_{23} & L^i_{25} & L^i_{26} \\ L^i_{43} & L^i_{45} & L^i_{46} \end{pmatrix} \tag{45}
$$

$$
{}^{TL}\mathbf{L}^i = \begin{pmatrix} L^i_{31} & L^i_{32} & L^i_{34} \\ L^i_{51} & L^i_{52} & L^i_{54} \\ L^i_{61} & L^i_{62} & L^i_{64} \end{pmatrix} \quad {}^{TT}\mathbf{L}^i = \begin{pmatrix} L^i_{33} & L^i_{35} & L^i_{36} \\ L^i_{53} & L^i_{55} & L^i_{56} \\ L^i_{63} & L^i_{65} & L^i_{66} \end{pmatrix}
$$

We also define some abbreviations

$$
\alpha^i = {}^{LL}\mathbf{L}^i - {}^{LT}\mathbf{L}^i : \left({}^{TT}\mathbf{L}^i\right)^{-1} : {}^{TL}\mathbf{L}^i \qquad \beta^i = {}^{LT}\mathbf{L}^i : \left({}^{TT}\mathbf{L}^i\right)^{-1} \tag{46}
$$

$$
\gamma^i = \left({}^{TT}\mathbf{L}^i\right)^{-1} : {}^{TL}\mathbf{L}^i \qquad \eta^i = \left({}^{TT}\mathbf{L}^i\right)^{-1}
$$

and their averages

$$
\alpha \equiv \sum_{j=1}^{N} c^j \alpha^j, \quad \beta \equiv \sum_{j=1}^{N} c^j \beta^j, \quad \gamma \equiv \sum_{j=1}^{N} c^j \gamma^j, \quad \text{and} \quad \eta \equiv \sum_{j=1}^{N} c^j \eta^j. \tag{47}
$$

Starting with the homogenisation Eq. (41) for the stress, and after rearrangement of the governing equations, we find expressions for all components of the stress in each layer i. Upon comparison with the TFA stress localisation of Eq. (8), we obtain

$$
\begin{aligned}
{}^{LL}\bar{\mathbf{B}}^i &= \alpha^i : \alpha^{-1} & {}^{LT}\bar{\mathbf{B}}^i &= \beta^i - \alpha^i : \alpha^{-1} : \beta \\
{}^{TL}\bar{\mathbf{B}}^i &= \mathbf{0} & {}^{TT}\bar{\mathbf{B}}^i &= \mathbf{1}
\end{aligned} \tag{48}
$$

and

$$
\begin{aligned}
{}^{LL}\bar{\mathbf{Q}}^{ij} &= \delta_{ij}\alpha^i - c^j \alpha^i : \alpha^{-1} : \alpha^j & {}^{LT}\bar{\mathbf{Q}}^{ij} &= \mathbf{0} \\
{}^{TL}\bar{\mathbf{Q}}^{ij} &= \mathbf{0} & {}^{TT}\bar{\mathbf{Q}}^{ij} &= \mathbf{0}
\end{aligned} \tag{49}
$$

Instead of using homogenisation of stress of Eq. (41), we may use its counterpart, the homogenisation of strain. Proceeding as before, we then arrive at

$$
{}^{LL}\bar{\mathbf{A}}^i = \mathbf{1} \qquad {}^{LT}\bar{\mathbf{A}}^i = \mathbf{0} \tag{50}
$$

$$
{}^{TL}\bar{\mathbf{A}}^i = \eta^i : \eta^{-1} : \gamma - \gamma^i \qquad {}^{TT}\bar{\mathbf{A}}^i = \eta^i : \eta^{-1}
$$

and

$$
{}^{LL}\bar{\mathbf{D}}^{ij} = \mathbf{0} \qquad {}^{LT}\bar{\mathbf{D}}^{ij} = \mathbf{0} \tag{51}
$$

$$
{}^{TL}\bar{\mathbf{D}}^{ij} = \delta_{ij}\gamma^i - c^j\eta^i : \eta^{-1} : \gamma^j \qquad {}^{TT}\bar{\mathbf{D}}^{ij} = \delta_{ij}\mathbf{1} - c^j\eta^i : \eta^{-1}
$$

We can now collect equations to write the equivalent of Eq. (39):

$$
\begin{array}{rl}
\text{Strain localisation tensors } \underset{\approx}{\mathbf{A}}^i & \text{collect Eqs. (50)} \\
\text{Stress localisation tensors } \underset{\approx}{\mathbf{B}}^i & \text{collect Eqs. (48)} \\
\text{Overall stiffness} & \mathbf{L}^g = \sum_i c^i \underset{\approx}{\mathbf{L}}^i : \bar{\underset{\approx}{\mathbf{A}}}^i \\
(\text{Eigenstress influence tensor}) : \mathbf{L}^i & \text{Eq. (49)} \\
\text{Eigenstrain influence tensor} & \text{Eq. (51)}
\end{array} \tag{52}
$$

which, together with Eq. (40) defines our meso→micro transition. We have now all the ingredients of the full three-scale model, as depicted in Fig. 1.

4. Simulations

This section presents two simulations. In the first section the meso→micro model is validated with respect to an earlier formulation, and with respect to a full FE calculation. Then, some three-scale simulations are carried out on Near Gamma, Duplex, Near Lamellar and Fully Lamellar microstructures. All simulations have been carried out with the module MultiMat of the FE-code Zébulon (Zébulon, 2002), in which (among others) the scale transitions of the previous sections have been incorporated.

4.1. Meso→micro

In this section, some calculations are carried out in order to reproduce the orientation dependence of the lamellar phase with respect to the loading direction, such as found experimentally (e.g. in Inui et al., 1992; Werwer and Cornec, 2000). The simulations have been carried out in two different manners: a FE calculation of *one* lamellar grain and the corresponding formulation of the Gélébart model in the TFA framework, as presented in the previous sections. These calculations have been compared to the original Gélébart model.

A three-dimensional representative volume element, containing only *one* lamellar grain, has been loaded uniaxially in tension and compression at a strain rate $\dot{\varepsilon} = 4 \times 10^{-4}\ \mathrm{s}^{-1}$. More precisely, this volume element is thought to represent a section of a few lamellae of a large (infinite) PST-crystal. In the FE calculation, the RVE is

represented in a cube (left in Fig. 2) with periodic boundary conditions on the displacements at all external surfaces. The cube consists of one layer α_2 ($c^{\alpha_2}=0.10$) and six layers γ (each $c^{\gamma}=0.15$), each corresponding to one orientation variant (Kishida et al., 1998). The loading direction has been varied by rotating the macroscopic stress tensor that is applied to the volume element by an angle ϕ around the x_3-axis, as depicted in the right Fig. 2. The mechanical response has been calculated for $\phi=0^\circ$, 31°, 51°, 68° and 90°.

Because of the periodic boundary conditions in the FE computational cell, and the manner in which the macroscopic stress tensor is applied, we are solving numerically a periodic localisation problem of an infinite multilayer, for which an exact solution exists. It is precisely this solution that has been treated in Section 3.2, and it is therefore expected that the two solutions coincide.

The tensors of elasticity are given in Table 1 and the parameters pertaining to the slip systems are as follows: because of the absence of any experimental information on the hardening matrix $h_{\alpha\beta}$ only self-hardening is taken into account, i.e. $h_{\alpha\beta}$ equals the unit matrix. The exponential of the second Eq. (37) has been dropped and replaced with linear hardening $r_\alpha=r_0+Q\gamma_\alpha$ for comparison with the original Gélébart model. In order to approach time-independent plasticity, $n=20$ and $K=0.05$ MPa. For the γ-phase, $r_0=50$ MPa for normal slip and twinning, and 200 MPa for superslip. All systems have $Q=50$ MPa, which is very small, but of the same order of magnitude as found elsewhere in the literature (for instance Werwer and Cornec, 2000, or Schlögl, 1997). For the α_2-phase, $r_0=330$ MPa for basal slip, 100 MPa for prism slip and 910 MPa for pyramidal slip. Again $Q=50$ MPa. The morphological orientation factors are 1.0 for longitudinal slip, 1.3 for mixed slip and 2.2 for transversal slip.

The curves of the three models are found to overlap. The stress–strain curves are displayed in Fig. 3 for the TFA model, for compression (continuous lines) and tension (dashed lines). For contrast, curves for a monocrystal of γ-TiA1 under compression (same material parameters except for the morphological factors which are all 1.0) have been included in the figure as well (dotted lines). The figure would be unchanged if we would have taken the curves from the FE model, or from the original Gélébart model. The quantities are displayed in their Von Mises equivalent in order to compare the different orientations. In the FE results it has been verified that the stress, total deformation and plastic deformation for each slip system is uniform in each lamella, thereby verifying an assumption in the Gélébart model and its corresponding TFA formulation (see Section 3.2).

The Gélébart model had already been parametrized such that it reproduces the orientation dependence of the onset of plasticity that is found experimentally

Table 1
Components of the tensors of elasticity (in GPa): experimental values of Tanaka et al. (1996a,b)

Component	L_{11}	L_{22}	L_{33}	L_{44}	L_{55}	L_{66}	L_{12}	L_{23}	L_{31}
α_2	175	175	220	43.2	62.6	62.6	88.7	62.3	62.3
γ	183	183	178	78.4	105	105	74.1	74.4	74.4

(Gélébart, 2002). Note that for some orientations there is an asymmetry between tension and compression. This is caused by the unidirectional nature of the twinning systems. This asymmetry disappears when the twinning systems are suppressed from the simulation (Gélébart, 2002).

4.2. Three-scale model

This section presents the first simulations with the full three-scale TFA-model, where the lamellar grain is described exactly as in the previous section, although its spatial orientation may vary. The calculations are carried out on the four "standard" microstructures: Near Gamma (NG), Duplex, Near Lamellar (NL) and Fully Lamellar (FL). The relative (mesoscopic) volume fractions of each microstructure

Table 2
Composition of the simulated microstructures (in vol.%)

Microstructure	α_2 (%)	γ (%)	(α_2 + γ) (%)
NG	5	95	–
Duplex	–	50	50
Near lamellar	–	5	95
Fully lamellar	–	–	100

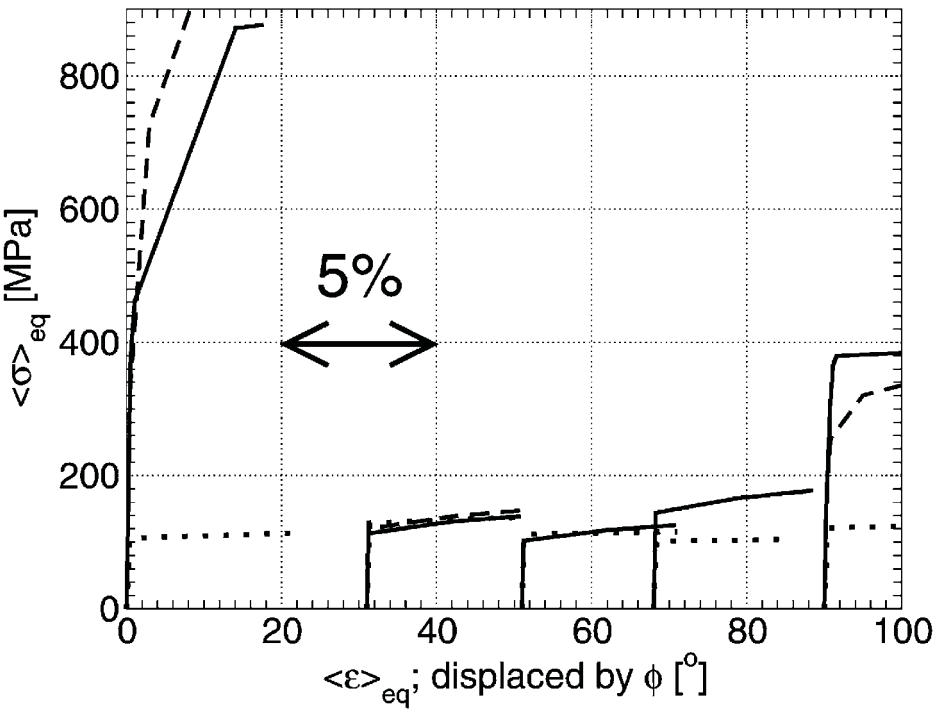

Fig. 3. Orientation dependence of the mesoscopic response of the lamellar grain under uniaxial compression (continuous lines) and tension (dashed lines). For contrast, corresponding curves for a γ-TiAl monocrystal have been added (dotted lines). The stresses and strains are given in Von Mises equivalents. The origins of the curves have been displaced along the horizontal axis according to their orientation angle ϕ, for clarity. The scale of the equivalent strain is indicated in the figure.

are given in Table 2, where each crystallographic orientation is represented with the same volume fraction. Note that since the NG microstructure in this table does not contain any lamellar grains, it is actually a classical polycrystal simulation, albeit with the generalisation of the Kröner model to anisotropic elasticity, Eq. (22). The microstructures consist of 40 grains which have random orientation. Each microstructure is based on the same composition, but all simulations have been carried out using four different realisations, i.e. with four different sets of random orientations.

As the aim of this section is only to show the viability of the method (instead of fitting to experimental data, which will be the subject of a future paper), some simplifications have been adopted. First, the simulations are carried out in one Gauss point at the macroscopic level. Then, each crystallographic orientation has the same volume fraction, i.e. no specific crystallographic texture is applied. No correction has been applied to correct for stiff Kröner behaviour, i.e. $D=0$ in Eq. (34). Finally, no verifications have been carried out whether 40 randomly oriented grains actually make up a representative sample of the actual microstructures. For grains with an isotropic mechanical response, one would typically use a few hundred of them. Given the strong anisotropic response of the lamellar grains, more would probably be needed here, and this would be straighforward to carry out. However, a systematic study is outside the scope of the present paper.

The grains are loaded under uniaxial tension or shear up to a few percent deformation at a strain rate $\dot{\varepsilon}=4\times10^{-4}$ s^{-1}. All material parameters are as in the previous section, except that for the monocrystalline grains, the morphological orientation factors do not come into play, i.e. they are all 1.0. The resulting macroscopic responses are displayed in Fig. 4, for two different loading conditions. Each curve is an average of four different realisations. The spread around each curve increases with increasing volume fraction of lamellar grains (not indicated in Fig. 4), and is of the order of 25 MPa (in both directions) for NG to 50 MPa for FL. It can be observed that macroscopic stress increases with increasing volume fraction of lamellar grains, which is qualitatively coherent with the strong anisotropy of the lamellar phase, as shown in the previous section.

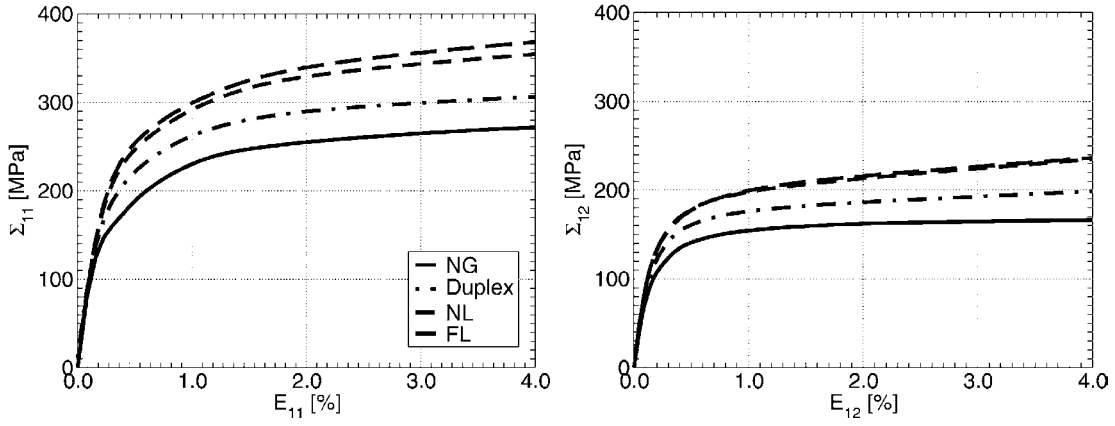

Fig. 4. Macroscopic responses under (left) uniaxial loading in the horizontal direction E_{11} (tension) and (right) shear E_{12}. Each curve represents an average of four independent realisations of the same type of microstructure.

5. Concluding remarks

In this work, a three-scale mechanical model for the deformation of titanium aluminides has been presented as depicted in Fig. 1. The model, that takes into account the typical length scales present in the different TiA1 microstructures, has been constructed within the framework of Transformation Field Analysis and of crystal plasticity. It consists of two scale transformations: a macro→meso transition between the structural scale and the scale of each individual grain, and a meso→micro transition for the lamellar grain down to each lamella. It has been shown that some existing approaches for these scale transformations can be written in the general framework of TFA.

In the first transition the grains are supposed to be spherical and embedded in an elastically self-consistent equivalent medium. Each grain is specified by its volume fraction and orientation. There are no assumptions on the type of elasticity. The second transition is equivalent to a multilayer model developed earlier by Gélébart et al. for the lamellar phase of TiA1. Again, each layer is specified by its volume fraction and orientation.

The meso→micro transition has been validated with respect to a full FE calculation and the Gélébart model. A lamellar grain, consisting of one layer α_2 and six layers γ, each oriented according to one of the six orientation relations found experimentally, has been subjected to uniaxial tension and compression in several directions with respect to the lamellar plane. The equivalent stress–equivalent strain curves of the three methods are found to coincide, as expected.

A simple simulation has been carried out to show the viability of the three-scale method. The three-scale simulation consisted 40 randomly oriented grains at the meso-level and the lamellar configuration as described above at the micro-level, for the four ''standard'' microstructures. The simulations show a trend towards increasing dispersion in the macroscopic response, and an increasing macroscopic stress with increasing volume fraction of lamellar grains. However, future work will have to look into such issues as representativity of the chosen microstructures in terms of orientation distributions, number of grains, etc. Currently, further simulations are carried out in order to adjust the material parameters to experimental curves of polycrystalline samples.

Acknowledgements

This work has been financially supported by the French Ministry of Defence (DGA), which is gratefully acknowledged.

References

Bornert, M., Bretheau, T., Gilormini, P., 2001. Homogénéisation en mécanique des matériaux, 1. Matériaux aléatoires élastiques et milieux périodiques. Hermes, Paris (Chapter 5).

Brockman, R.A., 2003. Analysis of elastic–plastic deformation in TiAI polycrystals. Int. J. Plasticity 19, 1749–1772.
Cailletaud, G., 1987. Une approche micromécanique phénoménologique du comportement inélastique des métaux. Thèse d'État, Université Pierre et Marie Curie, Paris.
Chaboche, J.L., Kruch, S., Maire, J.F., Pottier, T., 2001. Toward a micromechanics based inelastic and damage modeling of composites. Int. J. Plasticity 17, 411–439.
Dvorak, G.J., Benveniste, Y., 1992. On transformation strains and uniform fields in multiphase elastic media. Proc. R. Soc. Lond A437, 291–310.
Ei Omri, A., Fennan, A., Sidoroff, F., Hihi, A., 2000. Elastic-plastic homogenization for layered composites. Eur. J. Mech. A/Solids 19, 585–601.
Gélébart, L., 2002. Approche multi-échelles du comportement mécanique de l'alliage Ti-$Al_{48}Cr_2Nb_2$. PhD Thesis, École Polytechnique Palaiseau.
Inui, H., Oh, M.H., Nakamura, A., Yamaguchi, M., 1992. Room-temperature tensile deformation of polysynthetically twinned (PST) crystals of TiAl. Acta Metall Mater. 40, 3095–3104.
Inui, H., Kishida, K., Misaki, M., Kobayashi, M., Shiray, Y., Yamaguchi, M., 1995. Temperature dependence of yield stress, tensile elongation and deformation structure in polysynthetically twinned crystals of Ti-Al. Phil. Mag. A72 (6), 1609–1631.
Kishida, K., Inui, H., Yamaguchi, M., 1998. Deformation of lamellar structure in TiAI-Ti_3Al two-phase alloys. Phil. Mag. A78 (1), 1–28.
Marketz, W.T., Fischer, F.D., Clemens, H., 2003. Deformation mechanisms in TiAl inter-metallics—experiments and modelling. Int. J. Plasticity 19, 281–321.
Morvan, J.-M., Chaboche, J.-L., 1999. A self-consistent modelling of plasticity with application to the heterogeneous microstructure of TiAl. In: Proceedings of the Seventh International Symposium on Plasticity and Its Current Applications (Plasticity '99), Cancun, Mexico, pp. 185–188.
Schlögl, S., 1997. Micromechanical Modelling of the Deformation Behaviour of Camma Titanium Aluminides. Fortschrittberichte VDI, Reihe 18, No. 220.
Stupkiewicz, S., Petryk, H., 2002. Modelling of laminated microstractures in stress-induced martensitic transformations. J. Phys. Mech. Solids 50, 2303–2331.
Suquet, P., 1997. Continuum Micromechanics. CISM, Udine.
Tanaka, K., Ichitsubo, T., Inui, H., Yamaguchi, M., Koiwa, M., 1996a. Single-crystal elastic constants of γ-TiAl. Phil. Mag. Lett. 73, 71–78.
Tanaka, K., Okamoto, K., Inui, H., Minonishi, Y., Yamaguchi, M., Koiwa, M., 1996b. Phil. Mag A73, 1475.
Werwer, M., Cornec, A., 2000. Numerical simulation of plastic deformation and fracture in polysynthetically twinned (PST) crystals of TiAl. Comp. Mat. Sci. 19, 97.
Yoo, M.H., Fu, C.L., Lee, J.K., 1991. The role of twinning in brittle fracture of Ti-aluminides. Mat. Res. Soc. Symp. Proc. 213, 545–554.
Yoo, M.H., Zou, J., Fu, C.L., 1995. Mechanistic modelling of deformation and fracture behavior in TiA1 and Ti_3A1. Mat. Sc. Eng. A192/193, 14–23.
Zebulon, 2002. Available from <http://www.nwnumerics.com>.
Zghal, S., Naka, S., Couret, A., 1997. A quantitative TEM analysis of the lamellar microstructure in TiAl based alloys. Acta Mater. 45, 3005–3015.